

Stimulus-driven traveling solutions in continuum neuronal models with a general smooth firing rate function

G. Bard Ermentrout* Jozsi Jalics† Jonathan E. Rubin‡

October 31, 2009

Abstract

We examine the existence of traveling wave solutions for a continuum neuronal network modeled by integro-differential equations. First, we consider a scalar field model with a general smooth firing rate function and a spatio-temporally varying stimulus. We prove that a traveling front solution that is locked to the stimulus exists for a certain interval of stimulus speeds. Next, we include a slow adaptation equation and obtain a formula, which involves a certain adjoint solution, for the stimulus speeds that induce locked traveling pulse solutions. Further, we use singular perturbation analysis to characterize an approximation to the adjoint solution. Numerical simulations are used to illustrate the traveling fronts and pulses that we study and to gain further insight into the adjoint solution.

1 Introduction

Traveling waves in neural field models have been the subject of extensive mathematical investigation (reviewed in [6, 5]). The motive for the study of these waves comes from numerous experiments in brain slices. Putative roles for these waves are discussed in [7, 19]. Early work [3, 11] showed that it is possible to evoke propagation of traveling waves in brain slices that have been treated with drugs that block inhibition. Recently, experimentalists have become interested in the effects of heterogeneity and stimuli on these waves. For example, certain experiments examined the induction of traveling waves in cortical slices in which there were varying densities of cells [16, 4]. Reflections and

*Department of Mathematics, University of Pittsburgh, Pittsburgh, PA 15260; bard@math.pitt.edu

†Department of Mathematics and Statistics, Youngstown State University, Youngstown, OH 44555; jalics@math.yosu.edu

‡Department of Mathematics, University of Pittsburgh, Pittsburgh, PA 15260; rubin@math.pitt.edu

blocking of these waves occurs, as do changes in preferred directionality. Stimuli can have dramatic effects on waves. Xu et al. [20] show complex effects arising in visually evoked waves in rat cortex and more recently have shown that stimuli at two different locations can modulate the resulting waves ([18] and Xu, personal communication). Richardson et al. [17] showed that electrical fields could be used to block, speed up, and slow down evoked waves.

Neural field models represent reductions and approximations of more “realistic” conductance-based models with the advantage of being much easier to analyze. Recently, the emergence of traveling waves, and other spatiotemporal patterns, was shown to occur in a neural field model to which a spatiotemporally varying stimulus was applied [1, 9, 10]. As in much of the work in this area, a Heaviside firing rate function was used in these papers. This simplification allows for the derivation of closed form solutions to the relevant field equations and analytical stability analysis, yet biologically, it implies that at each moment in time, cells are either firing at a unique nonzero constant rate or are not firing at all. The objective of this work is to study the effects of a spatiotemporally varying stimulus on a neural field model with a more realistic, smooth firing rate function. More specifically, we impose a small stimulus, $\varepsilon I(x, t)$, where $0 < \varepsilon \ll 1$ and $I(x, t) = I(x - ct)$ for some constant speed c , and we consider for what c values the field is able to follow the stimulus, in the sense that it supports a traveling wave solution of the same speed.

We analyze both a scalar field model and a model with adaptation. In the former case, our results build on the work of Ermentrout and McLeod [8], who proved the existence of monotone traveling fronts for a neural field without spatiotemporally varying stimulation, in one of the few rigorous works in this area allowing for a general smooth firing rate function (see also [13, 14]). In the case with adaptation, we assume that the adaptation evolves slowly relative to the population firing rate and build on the singular perturbation construction of a traveling pulse solution done previously by Pinto and Ermentrout, in the absence of spatiotemporally dependent applied stimulation [15].

2 Traveling fronts for a scalar field equation

2.1 Existence

Consider a single-layer neuronal network model distributed over the real line with a small, spatiotemporally varying stimulus applied:

$$\partial u(x, t) / \partial t = -u(x, t) + \int_{-\infty}^{\infty} J(x - y) F(u(y, t)) dy + \varepsilon I(x, t). \quad (2.1)$$

Here, $u(x, t)$ denotes the mean membrane potential of a patch of tissue at position x and time t , $J(x)$ denotes the distance-dependent synaptic weight function that measures the strength of excitatory synaptic connections between neurons, $F(u)$ denotes the firing rate function that depends on the membrane potential u , and $\varepsilon I(x, t)$ denotes the small, spatiotemporally varying stimulus, where $0 < \varepsilon \ll 1$.

We consider the existence of a traveling front for (2.1) under the hypotheses on J, F given in [8]:

(H1) The function $J(x)$ is defined, even, nonnegative, and absolutely continuous on \mathbb{R} , with $J' \in L^1(\mathbb{R})$ and $\int_{-\infty}^{\infty} J(x) dx = 1$.

(H2) The function $F(x)$ is defined and continuously differentiable on $[0, 1]$, with $F' > 0$, $F'(0) < 1$, and $F'(1) < 1$. Moreover, the function $F(u) - u$ has precisely three zeros, at $u = 0, u = a$, and $u = 1$, with $0 < a < 1$.

To start, define the moving coordinate $\xi = x - ct$ and assume that the stimulus term I takes the form of a traveling front,

$$I(\xi) \rightarrow \begin{cases} 1, & \xi \rightarrow -\infty, \\ 0, & \xi \rightarrow \infty, \end{cases} \quad \text{and } I(\xi) \in (0, 1) \text{ for all } \xi; \quad (2.2)$$

relevant $I(\xi)$ may be monotone decreasing, but assuming that this property holds is not necessary. We seek a traveling front solution $u(x - ct) = u(\xi)$ of equation (2.1) with the same speed c as the stimulus. Note that if $\varepsilon = 0$, or equivalently if $I \equiv 0$, then the results in [8] yield the existence of a family of monotone decreasing traveling fronts $u_0(\xi) = U(\xi - \theta)$, parametrized by $\theta \in \mathbb{R}$ (corresponding to translation), with $u_0(\xi) \rightarrow 1$ as $\xi \rightarrow -\infty$ and $u_0(\xi) \rightarrow 0$ as $\xi \rightarrow \infty$, for a special speed $c = c_0$. We assume that

(H3) $\int_0^1 (F(u) - u) du \neq 0$,

such that $c_0 \neq 0$. The work in [8] can be used to establish the following result.

Proposition 2.1 *For the solution u_0 of equation (2.1) with $\varepsilon = 0$, $u'_0(\xi) \in L^2(\mathbb{R})$.*

proof: F and u_0 satisfy the equation ([8], pg. 465)

$$-c_0 \int_{-\infty}^{\infty} (u'_0)^2 F'(u_0) d\xi = \int_0^1 \{-u_0 + F(u_0)\} du_0,$$

so $\int_{-\infty}^{\infty} (u'_0)^2 F'(u_0) d\xi$ takes a nonzero finite value, say i_0 , by (H3). Moreover, by (H2), F' is strictly positive and continuous on $[0, 1]$, such that it has a positive lower bound, call it m . Thus, $i_0 > 0$ and $\int_{-\infty}^{\infty} (u'_0)^2 d\xi \leq i_0/m < \infty$, as desired. \square

To find traveling front solutions in the presence of the stimulus term $I(\xi)$, we rewrite equation (2.1) in a moving frame, up to first order in ε , as

$$-(c_0 + \varepsilon c_1) du/d\xi = -u + J(\xi) * F(u(\xi)) + \varepsilon I(\xi), \quad (2.3)$$

where $c = c_0 + \varepsilon c_1 + O(\varepsilon^2)$ and $u = u_0 + \varepsilon u_1 + O(\varepsilon^2)$. The following theorem characterizes traveling front solutions to equation (2.3).

Theorem 2.2 *Let u_0 denote the nontrivial traveling front solution to equation (2.1) with $\varepsilon = 0$ and let c_0 be the corresponding wave speed. There is a unique nontrivial function $u^* \in L^2(\mathbb{R})$ that satisfies the adjoint equation*

$$\mathcal{L}^* u^* := (c_0 d/d\xi + 1)u^* - F'(u_0(\xi))(J(\xi) * u^*(\xi)) = 0 \quad (2.4)$$

together with the normalization condition

$$\int_{-\infty}^{\infty} u^*(\xi) u'_0(\xi) d\xi = 1.$$

Moreover, equation (2.3) has a solution $u_0(\xi) + \varepsilon u_1(\xi)$, with

$$u_1(\xi) \rightarrow \begin{cases} 0, & \xi \rightarrow \infty \\ (1 - F'(1))^{-1} \in (1, \infty), & \xi \rightarrow -\infty, \end{cases} \quad (2.5)$$

if and only if $c_1 \in [0, C)$, where

$$0 < C := \sup_{\theta \in \mathbb{R}} \left(- \int_{-\infty}^{\infty} u^*(\xi - \theta) I(\xi) d\xi \right) \leq \bar{C} := - \int_{-\infty}^{\infty} u^*(\xi) d\xi. \quad (2.6)$$

proof: At lowest order in ε , equation (2.3) is satisfied by $u_0(\xi - \theta)$ for any choice of θ . At first order, for fixed $\theta \in \mathbb{R}$, the equation for u_1 becomes

$$-c_0 u_{1\xi} + u_1 - J(\xi) * [F'(u_0(\xi - \theta))u_1(\xi)] = c_1 u_{0\xi} + I(\xi). \quad (2.7)$$

Rewrite the left hand side of equation (2.7) as $\mathcal{L}u_1$ for $\mathcal{L} : L^2(\mathbb{R}) \rightarrow L^2(\mathbb{R})$. The operator \mathcal{L} has $u'_0(\xi - \theta) < 0$ in its nullspace, based on differentiation with respect to ξ of the equation satisfied by u_0 and application of Proposition 2.1. Hence, by the Fredholm Alternative, there exists $u^*(\xi - \theta)$, a nontrivial solution to the corresponding adjoint equation, $\mathcal{L}^*u = 0$, satisfying $u^* \in L^2(\mathbb{R})$.

Assuming that the solution u^* is sign-definite, it can be normalized such that

$$\int_{-\infty}^{\infty} u^*(\xi)u'_0(\xi) d\xi = 1, \quad (2.8)$$

and equation (2.7) has a solution if and only if

$$\langle u^*(\xi - \theta), c_1 u_{0\xi} + I(\xi) \rangle = 0. \quad (2.9)$$

Condition (2.9) is equivalent, based on the normalization (2.8) and the fact that $u_0(\xi)$ is monontone decreasing, to the condition

$$c_1 = - \int_{-\infty}^{\infty} u^*(\xi - \theta)I(\xi) d\xi \equiv S(\theta) > 0. \quad (2.10)$$

Thus, we expect to obtain a band of solutions, corresponding to c_1 values between the minimum and maximum values of $S(\theta)$. Based on the behavior of $I(\xi)$ assumed in (2.2), these values are 0 and $C \in (0, \bar{C}]$, as given in equation (2.6), respectively.

It remains to derive the adjoint equation (2.4) and to conclude that u^* is indeed sign-definite. If we write out the first order equation (2.7) in more detail, we see that

$$\langle \mathcal{L}u, v \rangle = \int_{-\infty}^{\infty} [(-c_0 d/d\xi + 1)u(\xi)]v(\xi) d\xi - \int_{-\infty}^{\infty} v(\xi) \int_{-\infty}^{\infty} J(\xi - \eta)F'(u_0(\eta - \theta))u(\eta) d\eta d\xi.$$

If we apply integration by parts to the first integral and rewrite the second by Fubini's Theorem, then we obtain

$$\langle \mathcal{L}u, v \rangle = \int_{-\infty}^{\infty} [(c_0 d/d\xi + 1)v(\xi)]u(\xi) d\xi - \int_{-\infty}^{\infty} u(\eta)[F'(u_0(\eta - \theta)) \int_{-\infty}^{\infty} J(\xi - \eta)v(\xi) d\xi] d\eta.$$

Hence, the relevant adjoint equation is

$$\mathcal{L}_\theta^* u^* := (c_0 d/d\xi + 1)u^* - F'(u_0(\xi - \theta))(J(\xi) * u^*(\xi)) = 0.$$

Theorem 4.3 of [8] implies that for any fixed $\theta \in \mathbb{R}$, this equation has a solution that is unique, up to multiplication by a nonzero constant, and is sign-definite, which justifies the normalization (2.8). Finally, equation (2.5) follows from taking $\xi \rightarrow \pm\infty$ in (2.7) and noting that $u_{1_\xi}(\pm\infty) = u_{0_\xi}(\pm\infty) = u_0(\infty) = I(\infty) = 0$, $u_0(-\infty) = 1$, $I(-\infty) = 1$, and $F'(1) < 1$. \square

Remark 2.3 Note that since u^* is sign-definite, the sign of c_1 is determined by the sign of the stimulus I . If I is replaced by $-I$, then the sign of c_1 switches but its magnitude remains unchanged. Thus, the theory shows that application of small stimuli can speed up or slow down traveling fronts by equal amounts. We shall see that this is not the case when adaptation is included in the model, in the next section.

2.2 A special case: comparison to previous results

Although it does not have a derivative with a positive bound for $u \in [0, 1]$, we formally consider the special case of a Heaviside firing rate, $F(u) = H(u - \kappa)$, so that we can compare Theorem 2.2 to previous results [10]. Without loss of generality, assume that $u_0(0) = \kappa$; that is, $\theta = 0$. In this case, the adjoint equation (2.4) formally becomes

$$c_0 w' + w = \delta(u_0(\xi) - \kappa) \int_{-\infty}^{\infty} J(\xi - \eta) w(\eta) d\eta. \quad (2.11)$$

To solve equation (2.11) for $w(\xi)$, use the integrating factor e^{ξ/c_0} and integrate to obtain

$$w(\xi) e^{\xi/c_0} = \frac{1}{c_0} \int_{-\infty}^{\xi} e^{\zeta/c_0} \delta(u_0(\zeta) - \kappa) \int_{-\infty}^{\infty} J(\zeta - \eta) w(\eta) d\eta d\zeta. \quad (2.12)$$

Since $\zeta \in (-\infty, \xi)$, it follows that $\delta(u_0(\zeta) - \kappa) \equiv 0$ for $\xi < 0$. Using this observation and switching the order of integration in (2.12) yields, for $\xi > 0$,

$$w(\xi) e^{\xi/c_0} = \frac{1}{c_0} \int_0^{\infty} \frac{J(\eta) w(\eta)}{|u_0'(0)|} d\eta \equiv B, \quad (2.13)$$

where B is a constant. That is, $w(\xi) = BH(\xi)e^{-\xi/c_0}$ for some constant B , where H as usual denotes the Heaviside step function.

To check the consistency of this solution, assume $\xi > 0$ and substitute it into both sides of equation (2.13) to obtain

$$B = \frac{B}{c_0} \int_0^\infty \frac{J(\eta)e^{-\eta/c_0}}{|u'_0(0)|} d\eta. \quad (2.14)$$

For consistency, the right hand side of equation (2.14) should equal B . This is indeed the case for the choice $J(x) = e^{-|x|}/2$ since, using the corresponding calculation

$$u'_0(\xi) = -e^{-\xi}/(2(1+c_0)) \quad (2.15)$$

from [8] or [10] evaluated at $\xi = 0$, we have

$$\frac{B}{c_0} \int_0^\infty \frac{J(\eta)e^{-\eta/c_0}}{|u'_0(0)|} d\eta = \frac{2B(1+c_0)}{c_0} \int_0^\infty \frac{1}{2} e^{-\eta} e^{-\eta/c_0} d\eta = \frac{B(1+c_0)}{c_0(1+\frac{1}{c_0})} = B,$$

as desired. Note that this solution of equation (2.4), applied for arbitrary θ , yields

$$w(\xi - \theta) = BH(\xi - \theta)e^{-(\xi-\theta)/c_0}. \quad (2.16)$$

Now, to compute B , we use the normalization equation (2.8), with $u^* = w$ from equation (2.16) and $u'_0(\xi)$ from equation (2.15), to obtain

$$1 = B \int_0^\infty e^{-\xi/c_0} u'_0(\xi) d\xi = -B \int_0^\infty e^{-\xi/c_0} \frac{e^{-\xi}}{2(c_0+1)} d\xi.$$

After some calculation, we find $B = -2(1+c_0)(\frac{1}{c_0}+1)$.

Finally, the speed term c_1 is given by equation (2.10). To compare to the speed obtained previously for a stimulus with $O(\varepsilon)$ amplitude [10], take $I(\xi) = I_0H(-\xi)$. Note that the lower bound for c_1 is 0, obtained from (2.10) for $\theta > 0$. For $\theta < 0$, (2.10) becomes

$$\begin{aligned} c_1 &= \int_{-\infty}^\infty 2(1+c_0)(\frac{1}{c_0}+1)H(\xi-\theta)e^{-(\xi-\theta)/c_0}I_0H(-\xi) d\xi \\ &= 2I_0(1+c_0)(\frac{1}{c_0}+1) \int_\theta^0 e^{-(\xi-\theta)/c_0} d\xi. \end{aligned} \quad (2.17)$$

Using the fact that $c_0 = (1-2\kappa)/(2\kappa)$ from [8], evaluation of this integral and some algebra yields

$$c_1 = \frac{I_0(1-e^{\theta/c_0})}{2\kappa^2}. \quad (2.18)$$

Thus, the upper bound for c_1 is $\frac{I_0}{2\kappa^2}$, which is approached as $\theta \rightarrow -\infty$. According to [10], the right boundary of the existence region in the (c, I_0) -plane is given by $c = \frac{1}{2(\kappa-\varepsilon I_0)} - 1$.

Note that this speed is approached as $\xi_0 \rightarrow -\infty$. Rewriting this expression for c as $c_0 + \varepsilon c_1$ with $c_0 = \frac{1}{2\kappa} - 1$ and solving for c_1 results in

$$c_1 = \frac{I_0}{2\kappa(\kappa - \varepsilon I_0)} = \frac{I_0}{2\kappa^2} + O(\varepsilon). \quad (2.19)$$

Consequently, our existence regions agree within $O(\varepsilon)$ to those of [10]; that is, for both techniques, $c \in [c_0 = \frac{1}{2\kappa} - 1, c_0 + \varepsilon(\frac{I_0}{2\kappa^2} + g(\kappa, I_0, \varepsilon))]$ where $g(\kappa, I_0, \varepsilon) = O(\varepsilon)$ and $0 < \kappa \leq 1/2$.

2.3 Numerical examples

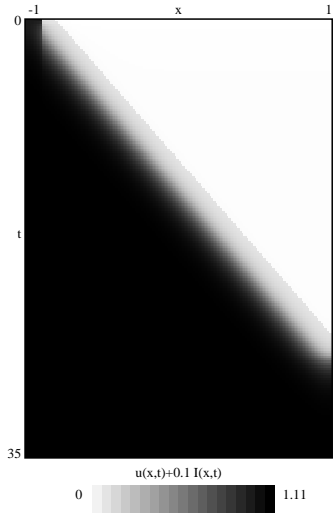
In this subsection, we present typical numerical simulations of equation (2.1). These results show examples of the successful propagation of traveling fronts that track moving stimuli as well as examples of failures to track. Of course, it is not possible to simulate (2.1) on the whole real line in space or time. For each example, we consider the domain $x \in [-1, 1]$ and we choose a stimulus function $I(\xi)$ and a relevant initial condition $u(x, 0)$ for $x \in [-1, 1]$. In some cases, we assume that the stimulus function $I(\xi)$ is the Heaviside step function $H(-\xi - b)$ for some choice of $b \in (0, 1)$ and $c > 0$, with $\xi = x - ct$, such that (2.2) is satisfied. To approximate the arrival of a traveling front solution of (2.1) to a particular interval of x values within a larger (e.g. infinite) spatial domain, we simulate with initial conditions $u(x, 0) > 0$ for x near -1 and $u(x, 0) = 0$ for all other $x \in [-1, 1]$. We predict that, for this initial configuration with stimulus $\varepsilon I(\xi)$ applied for small $\varepsilon > 0$, we will observe activity propagating in the direction of increasing x with speed c , the speed of the stimulus, if and only if c is sufficiently close to the interval $[c_0, c_0 + \varepsilon C]$, where C is given by equation (2.6). Similarly, we also consider stimuli $-\varepsilon I(\xi) = -\varepsilon H(-\xi - b)$, to follow up on Remark 2.3, and we expect to observe propagation on $(c_0 - \varepsilon C, c_0]$ in this case.

For our simulations, we use $F(u) = 1/(1 + \exp(-20u + 5))$ and $J(x) = 10 \exp(-20|x|)$ and normalize the natural, unstimulated wave speed to $c_0 = 1$. Consider first a simulation in which we start with u activated in the leftmost 5% of the domain by using initial conditions $u(x, 0) = .9H(-x - 0.9)$ and with the front of the stimulus, which will move with speed c , slightly ahead of the activated region, choosing $b = 0.8$ such that $I(x, 0) = H(-x - 0.8)$. We find that for a stimulus magnitude of $\varepsilon = 0.01$, the interval of speeds for which stimulus-locked traveling fronts exist is roughly $c \in [1, 1.2)$. For a stimulus speed of

$c = 1.1$, for example, the front that is initiated by the initial conditions succeeds in tracking closely behind the stimulus and propagating from left to right with the same speed as the stimulus front. This is illustrated in Figure 1(a), where we plot $u(x, t) + 10\varepsilon I(x, t)$ to show the close tracking of the wave front to the stimulus front. With all the same conditions and a faster stimulus speed of $c = 1.3$, the simulated wave front fails to keep up with the faster stimulus front, falling farther and farther behind as seen in Figure 1(b).

Next, we consider the case of a negative (inhibitory) stimulus of the same magnitude. That is, we replace $\varepsilon I(x, t)$ with $-\varepsilon I(x, t)$ and keep all other conditions the same, and we find that the existence interval for stimulus-locked traveling fronts is roughly $c \in [0.8, 1)$. This is consistent with our analysis that shows that two stimuli of the same magnitude but opposite sign can speed up or slow down traveling fronts by the same amount (see Remark 2.3). A successful stimulus-locked traveling front is shown in Figure 1(c) for $c = 0.9$ while a failure to track is shown in Figure 1(d) with $c = 0.7$, where $u(x, t) - 10\varepsilon I(x, t)$ is plotted in each case to show the relation of the traveling front to the stimulus front. We note that the successful, stimulus-locked fronts in Figures 1(a),1(c) correspond to the analytically computed traveling fronts. However, the front-like solutions in Figures 1(b),1(d) that do not lock to the stimulus do not represent true traveling wave solutions on the entire real line, but rather provide evidence that traveling wave solutions do not exist for those values of c outside of the existence interval.

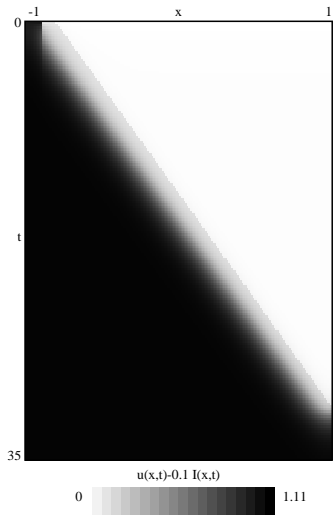
Remark 2.4 The particular interval of speeds c for which stimulus-induced wave propagation succeeds depends on the form of $I(\xi)$, in addition to its amplitude, as indicated in equation (2.6). For example, suppose we replace the Heaviside stimulus with a monotone increasing sigmoidal stimulus $I(\xi) = 1/(1 + \exp((-\xi - b)/\sigma))$, $\sigma > 0$. Successful stimulus tracking occurs on progressively larger intervals of c as σ increases. Tracking does not seem to be particularly sensitive to the particular value selected for b .



(a) $c=1.1$



(b) $c=1.3$



(c) $c=0.9$



(d) $c=0.7$

Figure 1: Stimulus-locked traveling fronts. (a),(c) Successful and (b),(d) failed propagation with (a),(b) $\varepsilon I(x, t) = 0.01H(-(x-ct)-0.8)$ and (c),(d) $\varepsilon I(x, t) = -0.01H(-(x-ct)-0.8)$. For these simulations, $F(u) = 1/(1 + \exp(-20u + 5))$ and $J(x) = 10 \exp(-20|x|)$.

3 Traveling pulses with slow adaptation

We now include a slow adaptation equation in the neural field model under consideration and seek to extend an earlier singular perturbation construction of a pulse solution [15] to allow for the inclusion of a small, spatiotemporally pulsatile stimulus. Unlike the analysis in Section 2.1, our approach here is not fully rigorous. In particular, we do not have sufficient information about the derivative of the pulse solution to draw rigorous conclusions about the existence and uniqueness of a solution to a relevant adjoint equation. We will nonetheless proceed formally to derive a formula for the stimulus speeds for which traveling pulses are predicted to exist. Furthermore, for numerical experimentation and more precise estimation of the stimulus speeds that can be tracked, we will consider solutions with the particular weight function $J(x) = \frac{1}{2}e^{-|x|}$ and approximate the homoclinic solution corresponding to the pulse solution with a large amplitude periodic solution.

With adaptation, the model equations that we consider become

$$\begin{aligned} \partial u(x, t)/\partial t &= -u(x, t) + \int_{-\infty}^{\infty} J(x-y)F(u(y, t)) dy - q(x, t) + \varepsilon I_a(x, t) \\ (1/\kappa)\partial q(x, t)/\partial t &= -\beta q(x, t) + u(x, t), \end{aligned} \quad (3.20)$$

where $0 < \kappa \ll 1$, $0 < \varepsilon \ll 1$, and $q(x, t)$ represents a negative feedback recovery mechanism such as spike frequency adaptation. We introduce the moving coordinate $\xi = x - ct$ and assume a pulsatile stimulus with $I_a(x, t) = I_a(\xi) \rightarrow 0$ as $\xi \rightarrow \pm\infty$. We seek traveling pulse solutions that are locked to the stimulus. Using our earlier notation for convolutions, traveling pulse solutions to (3.20) satisfy

$$\begin{aligned} -cu'(\xi) &= -u(\xi) + J * F(u(\xi)) - q(\xi) + \varepsilon I_a(\xi), \\ (-c/\kappa)q'(\xi) &= u(\xi) - \beta q(\xi), \end{aligned} \quad (3.21)$$

together with the boundary conditions $(u, q)(\xi) \rightarrow 0$ as $\xi \rightarrow \pm\infty$.

3.1 Fredholm alternative gives expression for relevant wavespeeds

Write $c = c_0 + \varepsilon c_1$, $u = u_0 + \varepsilon u_1$, $q = q_0 + \varepsilon q_1$ to leading order in the small parameter ε , with

$$u_1, q_1 \rightarrow 0 \text{ as } \xi \rightarrow \pm\infty. \quad (3.22)$$

With this notation, system (3.21) becomes

$$\begin{aligned} -(c_0 + \varepsilon c_1)(u_{0\xi} + \varepsilon u_{1\xi}) &= -(u_0 + \varepsilon u_1) + J * F(u_0 + \varepsilon u_1) - (q_0 + \varepsilon q_1) + \varepsilon I_a, \\ -(1/\kappa)(c_0 + \varepsilon c_1)(q_{0\xi} + \varepsilon q_{1\xi}) &= (u_0 + \varepsilon u_1) - \beta(q_0 + \varepsilon q_1). \end{aligned} \quad (3.23)$$

Since we know that a pulse $(u_0(\xi), q_0(\xi))$ exists in the unstimulated case with $\varepsilon = 0$ from [15], we solve for the $O(\varepsilon)$ correction terms introduced by the stimulus. At $O(\varepsilon)$, we find

$$\begin{aligned} -c_1 u_{0\xi} - c_0 u_{1\xi} &= -u_1 + J * F'(u_0)u_1 - q_1 + I_a \\ -(1/\kappa)(c_1 q_{0\xi} + c_0 q_{1\xi}) &= u_1 - \beta q_1. \end{aligned} \quad (3.24)$$

Rewrite equation (3.24) as

$$\begin{aligned} \mathcal{L}_a \begin{pmatrix} u_1 \\ q_1 \end{pmatrix} &:= \begin{pmatrix} -c_0 u_1' + u_1 - J(\xi) * F'(u_0)u_1 + q_1 \\ -c_0 q_1'/\kappa - u_1 + \beta q_1 \end{pmatrix} = \begin{pmatrix} c_1 u_0' + I_a \\ c_1 q_0'/\kappa \end{pmatrix} \\ &= \begin{pmatrix} I_a \\ 0 \end{pmatrix} + c_1 \begin{pmatrix} u_0' \\ q_0'/\kappa \end{pmatrix}. \end{aligned} \quad (3.25)$$

Let $(u^*(\xi - \theta), q^*(\xi - \theta))$ denote any solution to the adjoint equation $\mathcal{L}_a^* \begin{pmatrix} u^* \\ q^* \end{pmatrix} = 0$, parameterized by $\theta \in \mathbb{R}$, corresponding to translation invariance of traveling wave solutions of (3.20). According to the Fredholm alternative, system (3.25) has a nontrivial solution if and only if for some such (u^*, q^*) ,

$$\int_{-\infty}^{\infty} c_1(u_0'(\xi)u^*(\xi - \theta) + q_0'(\xi)q^*(\xi - \theta)/\kappa)d\xi + \int_{-\infty}^{\infty} I_a(\xi)u^*(\xi - \theta)d\xi = 0.$$

Normalizing such that

$$\int_{-\infty}^{\infty} (u_0'(\xi)u^*(\xi - \theta) + q_0'(\xi)q^*(\xi - \theta)/\kappa)d\xi = 1 \quad (3.26)$$

yields the result that traveling pulses exist for speeds $c = c_0 + \varepsilon c_1 + O(\varepsilon^2)$, where

$$c_1 = - \int_{-\infty}^{\infty} I_a(\xi)u^*(\xi - \theta)d\xi. \quad (3.27)$$

Remark 3.1 In subsection 3.2, we approximate the traveling pulse by a singular periodic orbit consisting of segments along a slow manifold and fast jumps between these segments. The adjoint solution corresponding to this periodic orbit is unique up to constant multiplication, suggesting that the nontrivial solution (u^*, q^*) of $\mathcal{L}_a^* \begin{pmatrix} u^* \\ q^* \end{pmatrix} = 0$, appearing in equations (3.26), (3.27), is unique as well.

Remark 3.2 Our subsequent calculations, in subsection 3.2, and numerical simulations, in subsection 3.3, illustrate that u^* need not be sign-definite, unlike the case of traveling fronts without adaptation. Hence, in the presence of a particular stimulus, waves may exist for an interval of speeds that is not symmetric about the unstimulated speed c_0 .

3.2 Behavior of the solution to the adjoint equation

To gain more information about our estimate of c_1 , given by equation (3.27), we seek to characterize the behavior of nontrivial solutions (u^*, q^*) to the adjoint equation corresponding to (3.25). To do so, it is convenient to approximate the traveling pulse solution by a periodic orbit of large period, so that we can use certain theoretical results obtained for adjoint solutions to such periodic solutions. Previous work has established that the singular perturbation construction of traveling pulses to a reaction-diffusion analogue of (3.20) on the real line, in the absence of stimulation, generalizes directly to give the existence of a periodic solution on a finite spatial domain with periodic boundary conditions [2]. Indeed, the argument for the existence of traveling pulses in [15] shows how to generalize the construction in [2] to the unstimulated form of (3.20), and the extension to the periodic case follows immediately.

Let $w = J * F(u)$, the convolution term from system (3.20). We will consider the special case of

$$J(x) = \frac{1}{2}e^{-|x|}, \quad (3.28)$$

such that application of the Fourier transform yields $\hat{w}(k) = [\hat{F}(u)](k)/(1 + k^2)$. In this case, $[\hat{F}(u)](k) = (1 + k^2)\hat{w}(k)$, such that inversion of the Fourier transform gives $F(u) = w - w''$, for $' = d/d\xi$. With this notation in place, traveling pulse solutions to the unstimulated form of (3.20), namely solutions to (3.21) with $\varepsilon = 0$, correspond to homoclinic solutions of

$$\begin{aligned} -cu' &= -u + w - q \\ -cq' &= \kappa(u - \beta q) \\ w' &= z \\ z' &= w - F(u), \end{aligned} \quad (3.29)$$

with $0 < \kappa \ll 1$. We seek periodic solutions of this system that approximate the homoclinic solution. We will also use the fast subsystem defined from (3.29) by setting $\kappa = 0$, which

consists of the u, w, z equations from (3.29) together with $q' = 0$, such that q is constant.

The slow formulation of system (3.29) is

$$\begin{aligned}
 -c\kappa\dot{u} &= -u + w - q \\
 -c\dot{q} &= u - \beta q \\
 \kappa\dot{w} &= z \\
 \kappa\dot{z} &= w - F(u),
 \end{aligned}
 \tag{3.30}$$

where differentiation is with respect to $\zeta = \kappa\xi$. The singular slow flow for this system is given by setting $\kappa = 0$ in (3.30), to obtain

$$-c\dot{q} = u - \beta q. \tag{3.31}$$

This flow is relevant on the slow manifold \mathcal{S} defined by $u - w + q = 0, z = 0, w = F(u)$, or equivalently $\{(u, q, w, z) : z = 0, q = F(u) - u\}$, in the $\kappa \rightarrow 0$ limit. Projected to (u, q) space, \mathcal{S} takes the form shown in Figure 2, and a singular periodic solution should be defined in the direction indicated by the arrows in the figure, given that $d/d\zeta = (-1/c\kappa)(d/dt)$, if we consider the case $c > 0$.

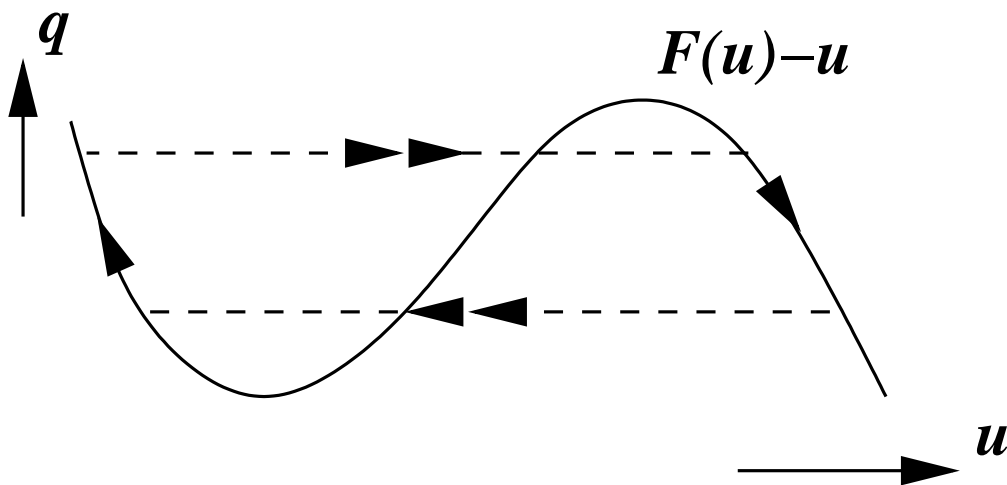


Figure 2: A schematic illustration of the projection of the slow manifold \mathcal{S} and the singular periodic solution to (u, q) space.

Before we proceed further, we make two important observations. First, note that the adjoint system to (3.29), reordered to put the slow q equation last, is

$$(x^*)' = M^*x^*, \tag{3.32}$$

where $x^* = [u^* \ w^* \ z^* \ q^*]^T$ and

$$M^* = \begin{bmatrix} -1/c & 0 & F'(u) & \kappa/c \\ 1/c & 0 & -1 & 0 \\ 0 & -1 & 0 & 0 \\ -1/c & 0 & 0 & -\beta\kappa/c \end{bmatrix}. \quad (3.33)$$

If we instead directly consider the equation $\mathcal{L}_a \begin{pmatrix} u \\ q \end{pmatrix} = 0$, with \mathcal{L}_a from (3.25), then the corresponding adjoint equations are

$$\begin{aligned} (u^*)' &= (F'(u)J * u^* - u^* + \kappa q^*)/c, \\ (q^*)' &= (-u^* - \kappa\beta q^*)/c. \end{aligned}$$

Now, let $z^* = (J * u^*)/c$. Using the form of J given in (3.28), the Fourier transform yields $\hat{u}^*(k) = c(1 + k^2)\hat{z}^*(k)$, such that $u^*/c = z^* - (z^*)''$. Finally, if we set $w^* = -(z^*)'$, then we recover the adjoint system (3.32), (3.33). Thus, the (u^*, q^*) components to solutions to the adjoint equations for system (3.29) satisfy the adjoint equation $\mathcal{L}_a^* \begin{pmatrix} u^* \\ q^* \end{pmatrix} = 0$ that is relevant for speed estimation through equations (3.26), (3.27) and vice versa.

By construction, solutions of (3.21) with $\varepsilon = 0$ satisfy system (3.29). The second observation that we make here is that all solutions to (3.29) also satisfy (3.21) with $\varepsilon = 0$. This can be seen by direct solution of the equation $w'' - w = -F(u)$ with variation of parameters. Indeed, when done on the real line, for example, this calculation yields $w(\xi) = \frac{1}{2} \int_{-\infty}^{\infty} F(u(\eta))e^{-|\eta-\xi|} d\eta = J * F(u)$, as desired.

Next, we would like to apply Theorem A.1 from [12] to characterize the limit to which the solution $(u^*(\zeta), q^*(\zeta), w^*(\zeta), z^*(\zeta))$ to the adjoint equations (3.32),(3.33), expressed with respect to the slow time $\zeta = \kappa\xi$, tends as the singular perturbation parameter $\kappa \downarrow 0$. As it is stated, this theorem applies to a relaxation oscillation solution that, in the singular limit, makes fast jumps from the knees of an underlying cubic-shaped slow manifold. The theorem provides explicit formulas for the jumps in the components of the adjoint solution that occur when the underlying relaxation oscillation jumps up and down. These formulas depend on the direction tangent to which the jumps originate. This direction is given by a left eigenvector of the Jacobian matrix of a fast subsystem, corresponding to the eigenvalue $\lambda = 0$ that exists precisely at the knees. In our notation, the knees are those points on \mathcal{S} such that $F'(u) = 1$. However, since we consider a traveling pulse solution, the relevant jumps do not occur where $F'(u) = 1$. Nonetheless, we can easily generalize the theorem

and its formulas by picking out the tangent eigenvector to the jump directions. Further details of the relevant calculations are given in the appendix.

Let $u = g_\alpha(q)$ denote the solutions to $q = F(u) - u$ on the left branch of \mathcal{S} , with $\alpha = L$, and on the right branch of \mathcal{S} , with $\alpha = R$. Implicit differentiation on \mathcal{S} yields

$$1 = (F'(g_\alpha(q)) - 1)g'_\alpha(q). \quad (3.34)$$

On \mathcal{S} , the slow flow (3.31) becomes

$$\dot{q} = (\beta q - g_\alpha(q))/c.$$

Moreover, from the slow formulation of (3.32),(3.33) in the $\kappa \rightarrow 0$ limit and equation (3.34), it follows that the corresponding slow adjoint equation is

$$\dot{q}^* = -(\beta/c)q^* + (1/c)g'_\alpha(q)q^*, \quad (3.35)$$

with corresponding normalization condition [12]

$$q^*(\beta q - g_\alpha(q))/c = 1. \quad (3.36)$$

Assume that a periodic orbit of system (3.30) has period ζ_p , let $\zeta_1 < \zeta_2 \in (0, \zeta_p)$ denote the two jump times associated with the orbit, and suppose that each jump takes off from a point a_j and lands at a point b_j . For any function f , let $f(\zeta_j^-) = \lim_{\zeta \uparrow \zeta_j} f(\zeta)$ and $f(\zeta_j^+) = \lim_{\zeta \downarrow \zeta_j} f(\zeta)$. The generalization of Theorem A.1 of [12] implies (see the appendix) that

$$q^*(\zeta_j^+) = q^*(\zeta_j^-) - c \left(\frac{G(b_j) - G(a_j)}{G(a_j)G(b_j)} \right), \quad j = 1, 2, \quad (3.37)$$

where $G(x) = (\beta q - g_\alpha(q))|_{(u,q,w,z)=x}$. Moreover,

$$\begin{bmatrix} u^* \\ w^* \\ z^* \end{bmatrix}(\zeta) = \begin{bmatrix} 1/(1 - F'(u)) \\ 0 \\ 1/(c(1 - F'(u))) \end{bmatrix} q^*(\zeta) + \begin{bmatrix} c^2 \\ c\lambda/(1 - \lambda^2) \\ c/(1 - \lambda^2) \end{bmatrix} \left(\frac{G(b_j) - G(a_j)}{G(a_j)G(b_j)} \right) \delta(\zeta - \zeta_j), \quad (3.38)$$

where λ is a certain eigenvalue of the Jacobian matrix of the fast subsystem of (3.29). Since we are not concerned with the jumps in w^* , z^* , we do not give an explicit formula for λ . Importantly, our original hypothesis that $F' > 0$, within (H2), implies that $\lambda \neq 1$; see the appendix for further details.

Remark 3.3 A transversality assumption is made in Theorem A.1 of [12] that here amounts to $\lambda \neq 1$. In fact, we shall see in the Appendix that $\lambda \neq 1$ is guaranteed by our assumption that $F'(u) \neq 0$.

At the jump up of the periodic solution,

$$\frac{G(b_1) - G(a_1)}{G(a_1)G(b_1)} = \frac{g_L(q(\zeta_1)) - g_R(q(\zeta_1))}{(\beta q(\zeta_1) - g_L(q(\zeta_1)))(\beta q(\zeta_1) - g_R(q(\zeta_1)))} > 0, \quad (3.39)$$

which yields $q^*(\zeta_1^+) < q^*(\zeta_1^-)$ from (3.37). At the jump down,

$$\frac{G(b_2) - G(a_2)}{G(a_2)G(b_2)} = \frac{g_R(q(\zeta_2)) - g_L(q(\zeta_2))}{(\beta q(\zeta_2) - g_R(q(\zeta_2)))(\beta q(\zeta_2) - g_L(q(\zeta_2)))} < 0, \quad (3.40)$$

which yields $q^*(\zeta_2^+) > q^*(\zeta_2^-)$. Between these jumps, q^* experiences an exponential ζ -dependence, as specified by equation (3.35). The magnitudes and signs of the jumps in u^* , namely $u^*(\zeta_i^+) - u^*(\zeta_i^-)$ for $i = 1, 2$, will depend on the comparison of $F'(u(\zeta_i^+))$ with $F'(u(\zeta_i^-))$, as specified in equation (3.38). Interestingly, it can also be seen from equations (3.38), (3.39), (3.40) that in the singular limit, the signs of the δ -function excursions of u^* at the two jumps will be in opposite directions.

3.3 Numerics

In theory, equations (3.37)–(3.40), together with the exponential behavior of q^* between jumps as given by (3.35), characterize the function $u^*(\xi - \theta)$ for any fixed θ , and hence fix the speed c_1 through equation (3.27). In this subsection, we first consider some numerical simulations of traveling pulse solutions of (3.20), and then we turn to some simulations that illustrate further properties of u^* .

As in the 1-d case, we work on $x \in [-1, 1]$, and we retain the same functions F and J used in Section 2.3, but we now assume that each stimulus function is a hat-shaped pulse with $\varepsilon I(\xi) = I_0 H(-\xi - 0.8) H(\xi + 1)$ for $I_0 \in \{\pm 0.01, \pm 0.05\}$ for some choice of $c > 0$ and $\xi = x - ct$. Also, in (3.20) we choose $\beta = 0$ and $\kappa = 0.15$ as in Figure 7 of [15]. The parameters used yield an unstimulated pulse speed of $c_0 = 1$. We activate the leftmost 5% of the domain with initial conditions $u(x, 0) = .7H(-x - 0.9)$ and initiate the stimulus pulse with its leading edge at $x = -0.8$, slightly ahead of the activated region. With $I_0 = 0.05$ and a stimulus speed of $c = 1.7$, for example, the pulse that is initiated

by the initial conditions appears to succeed in tracking closely behind the stimulus and propagating from left to right with the same speed as the stimulus pulse. This result is illustrated in Figure 3(a), where we plot $u(x, t) + 4\epsilon I(x, t)$ to show the close tracking of the wave pulse to the stimulus pulse. With all the same conditions and a faster stimulus speed of $c = 1.8$, the simulated wave pulse fails to keep up with the faster stimulus pulse, as shown in Figure 3(b).

For the negative (inhibitory) stimulus pulse and all other conditions unchanged, successful stimulus-locked traveling pulses are shown in Figures 4(a),4(c) for $c = 1.3$ and $c = 0.7$, respectively. Failures to obtain stimulus-locked pulses are shown in Figures 4(b),4(d) with $c = 1.5$ and $c = .65$, respectively. In Figure 4, $u(x, t) - 4\epsilon I(x, t)$ is plotted in each case to show the relation of the traveling pulse to the stimulus pulse.

As in the 1-d case with fronts, we note that the successful stimulus-locked pulses in Figures 3-4 correspond to traveling pulses on the real line, while the pulse-like solutions that fail to lock to the stimulus do not represent true traveling pulse solutions on the real line, but rather provide evidence that traveling pulse solutions do not exist for those values of c outside of the existence interval. Also as in the case of fronts, successful stimulus tracking occurs over larger intervals of speeds for stimuli that are sigmoidal approximations to the Heaviside function, with interval size growing as the slope of the sigmoid decreases. Unlike the fronts case, we find that for a fixed I_0 , pulses can track various stimuli with speeds that are slower or faster than the unstimulated speed, consistent with the idea that u^* is not sign-definite in equation (3.27). It is difficult to judge by inspection just when successful stimulus tracking is or is not occurring in our simulations, particularly since we are restricted to a domain of finite size. However, when the magnitude of I_0 decreases, say from 0.05 to 0.01, the interval of speeds for which stimulus-locked traveling pulses exist shrinks and appears to approach the form $(c_0 - a, c_0 + b)$, $a, b > 0$ for $I_0 > 0$ and $(c_0 - b, c_0 + a)$ for $-I_0 < 0$, again consistent with equation (3.27) and Remark 3.2.

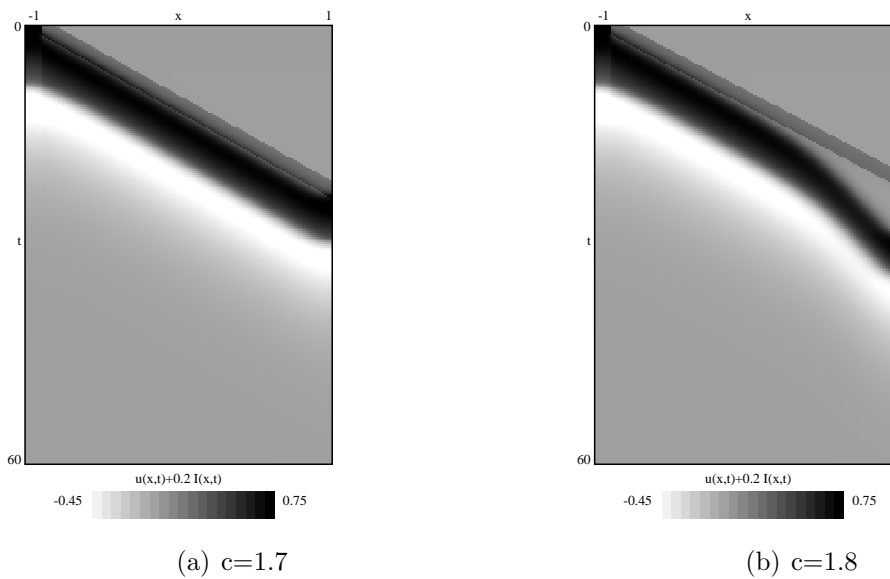


Figure 3: Stimulus-locked traveling pulses with stimuli of positive amplitude. (a) Success and (b) failure of propagation with $\varepsilon I(x, t) = 0.05H(-(x - ct) - 0.8)H(x - ct + 1)$ and (a) $c = 1.7$ or (b) $c = 1.8$. For these simulations, $F(u) = 1/(1 + \exp(-20u + 5))$, $J(x) = 10 \exp(-20|x|)$, $\beta = 0$, and $\kappa = 0.15$.

Recall that we have done calculations based on periodic solutions of system (3.29) to approximate the homoclinic traveling wave solutions. Correspondingly, we also consider periodic solutions numerically. Figure 5 shows an example of a periodic solution of system (3.29), projected onto (u, q) -space, together with the slow manifold \mathcal{S} and the graph of $(u, F(u))$. To find this periodic orbit, we used shooting with time reversed, because the spectrum of the linearization of the system features three positive and one negative eigenvalues in forward time. These become one positive and three negative eigenvalues in reversed time, rendering the shooting problem more tractable.

Numerically, we have computed u^*, q^* for the reversed time periodic orbit in Figure 5. Equation (3.40) yields a positive quantity with time reversed, since both the numerator and denominator are negative. Thus, from equation (3.37), we expect that q^* will decrease across the reversed time jump down, and this is what is observed numerically. Similarly, equation (3.39) yields a negative quantity with time reversed, and we indeed observe an increase in q^* across the reversed time jump up.

In this example, the take-offs and landings of both jumps occur from points where $F'(u) \approx 0$. Hence, we expect that each jump in u^* will be of a very similar magnitude to that in q^* , since equation (3.38) implies that

$$u^*(\zeta_i^+) - u^*(\zeta_i^-) = \left(\frac{1}{1 - F'(u(\zeta_i^+))} \right) q^*(\zeta_i^+) - \left(\frac{1}{1 - F'(u(\zeta_i^-))} \right) q^*(\zeta_i^-) \approx q^*(\zeta_i^+) - q^*(\zeta_i^-); \quad (3.41)$$

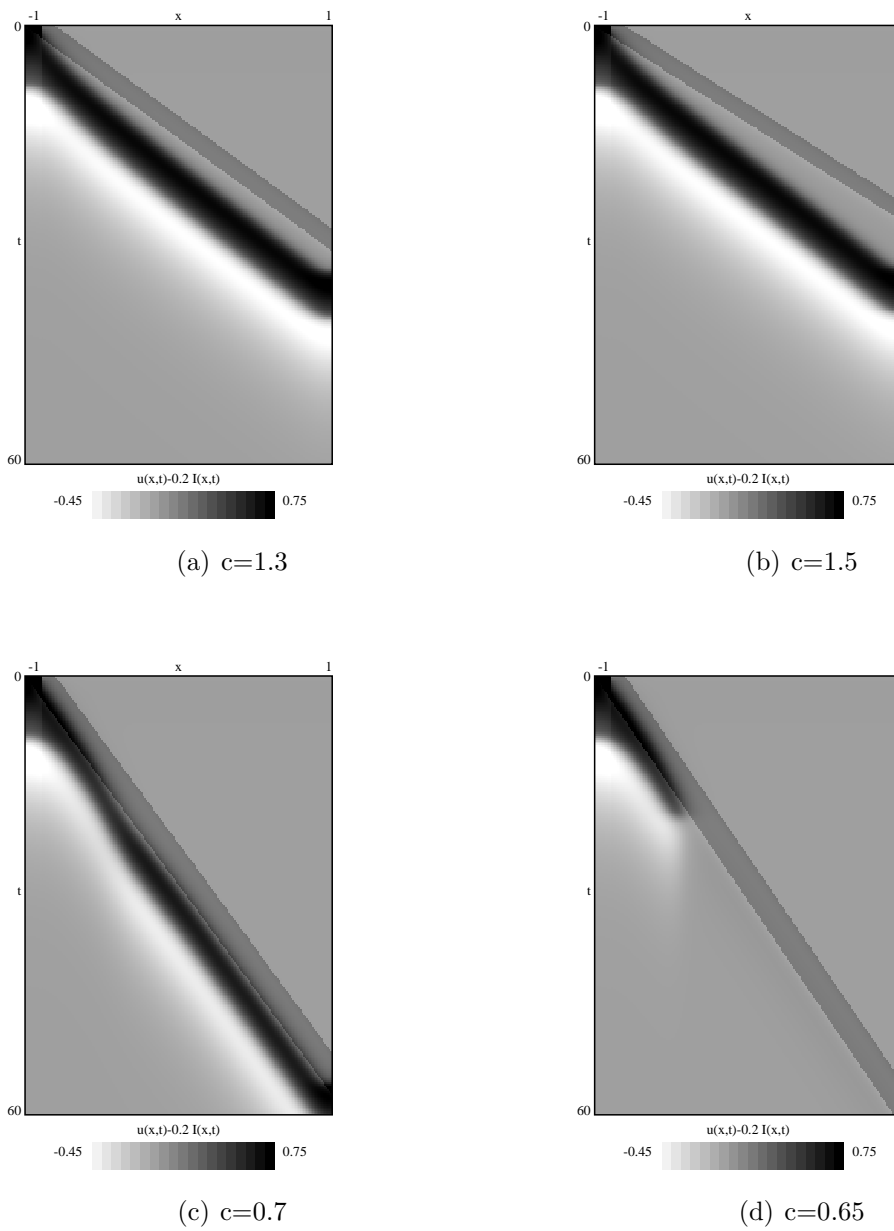


Figure 4: Stimulus-locked traveling pulses with stimuli of negative amplitude. (a),(c) Successful and (b),(d) failed propagation under the same conditions illustrated in Figure 3 except $\varepsilon I(x, t) = -0.05H(-(x - ct) - 0.8)H(x - ct + 1)$.

in particular, each jump in u^* are predicted to be in the same direction as the corresponding jump in q^* for $F'(u(\zeta_i^\pm))$ small.

More precisely, note (see also Figure 2 and Figure 6) that for each jump, the landing point is closer to a knee of \mathcal{S} than is the corresponding take off point. In reversed time, we thus have $F'(u(\zeta_i^+)) < F'(u(\zeta_i^-))$ for each i . Since $q^*(\zeta_2^+) < q^*(\zeta_2^-)$ from equations (3.37) and (3.40) with time reversed, it therefore follows from equation (3.41) that $u^*(\zeta_2^+) < u^*(\zeta_2^-)$. On the other hand, since $q^*(\zeta_1^+) > q^*(\zeta_1^-)$ from equation (3.39) with time reversed, equation (3.41) does not allow us to analytically guarantee the direction of the jump in

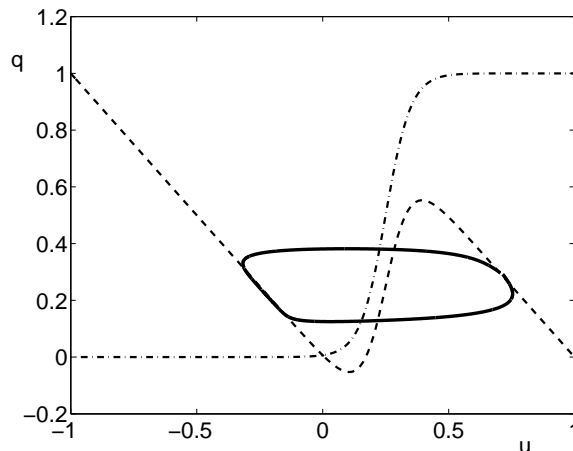


Figure 5: Estimated periodic solution of (3.29) (solid), slow manifold \mathcal{S} (dashed), and graph of $(u, F(u))$ (dash-dotted) projected into the (u, q) plane. Here, $c = .38, \kappa = .02, \beta = .25, F(u) = 1/(1 + \exp(-20u + 5))$. The flow along the periodic orbit is clockwise.

u^* at ζ_1 . Numerically, both jumps in u^* are indeed in the same directions as the jumps in q^* , as expected from (3.41) with $F'(u)$ small. Moreover, the δ -function excursions of u^* , with time reversed, are positive at the jump down and negative at the jump up, as predicted from equation (3.38), given the time reversed inequalities $q^*(\zeta_2^+) < q^*(\zeta_2^-)$ and $q^*(\zeta_1^+) > q^*(\zeta_1^-)$ noted above.

4 Conclusions

In this work, we have considered the existence of traveling solutions in continuum neuronal models that include a propagating applied stimulus $\varepsilon I(x, t) = \varepsilon I(x - ct)$, where the amplitude parameter ε is small. We work with two forms of neuronal models, one lacking adaptation that yields traveling front solutions and another with adaptation that supports traveling pulse solutions. Past work by Folias and Bressloff analyzed traveling solutions in stimulated neuronal media with Heaviside firing rate functions [1, 9, 10]. Papers by Ermentrout and McLeod [8] and Pinto and Ermentrout [15] considered the existence of traveling front and pulse solutions, respectively, in related models with more general, smooth firing rate functions, in the absence of spatiotemporally dependent applied stimulation. The current paper brings together these research directions, allowing for smooth firing rate functions in the stimulated case.

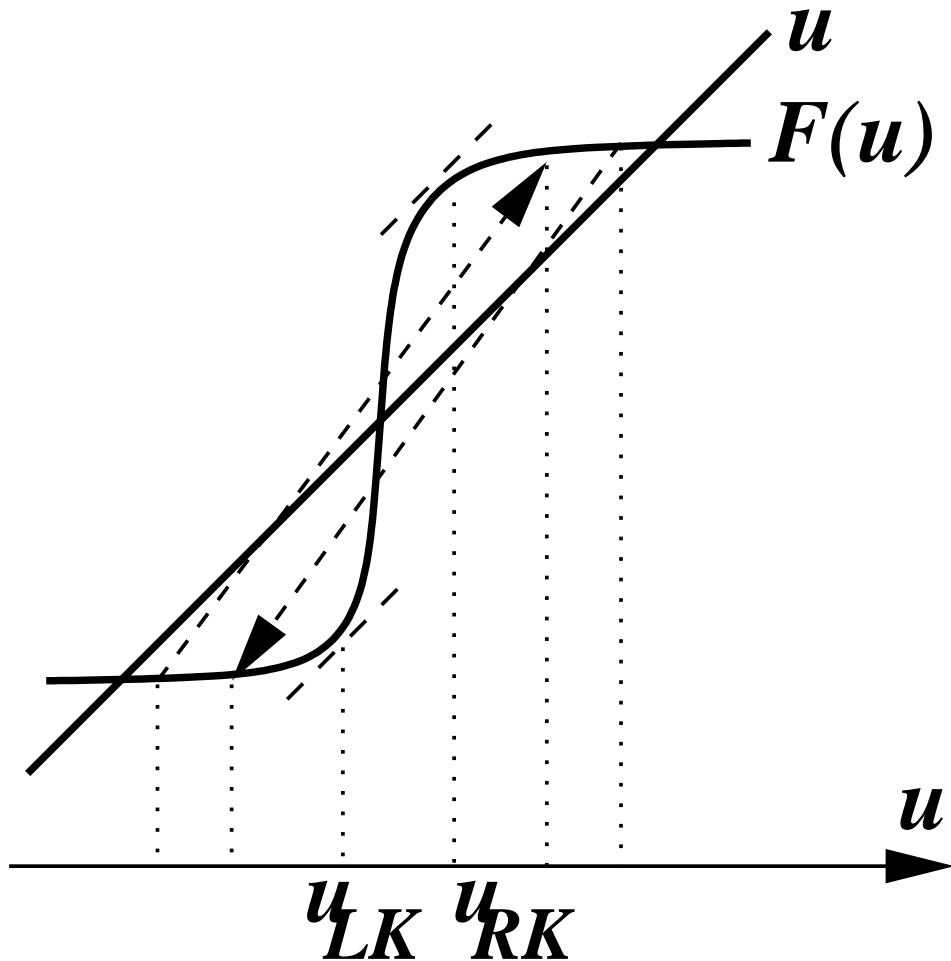


Figure 6: Illustration of $F'(u)$ at jump points. The knees of \mathcal{S} occur at the values $u = u_{LK}$ and $u = u_{RK}$, where $F'(u) = 1$, as indicated by the corresponding dashed segments. The directions of the jumps up and down are illustrated by the dashed lines with arrows. The jump up shown here occurs in the direction of increasing u , from a point below u_{LK} to a point above, but closer to, u_{RK} , leading to an increase in $F'(u)$ across the jump. The jump down occurs in the direction of decreasing u , from a point above u_{RK} to a point below, but closer to, u_{LK} , also leading to an increase in $F'(u)$ across the jump.

Our analysis shows that the Fredholm Alternative can be used to leverage the existence of a traveling solution in a model lacking stimulation to ascertain the existence of a related, stimulus-locked traveling solution when a small amplitude stimulus is applied. The range of speeds over which a solution exists, corresponding to successful tracking of the stimulus, can be estimated using this approach and depends on the form of the stimulus, although a general upper bound that does not depend strongly on this form can be derived in the traveling front case. This range of speeds also depends on the properties of a solution to an adjoint equation. We were not able to fully characterize the relevant adjoint solutions, but we do discuss theoretical and numerical results that clarify some of their properties as well as numerical examples illustrating the intervals of speeds over which twaves successfully track propagating stimuli. Interestingly, the analysis and simulations show that the nature of these intervals differs between the case of a traveling front stimulus in a model lacking neuronal adaptation and the case of a traveling pulse stimulus in a model including adaptation. In particular, in the case with adaptation, a stimulus of positive amplitude can induce a traveling pulse with speed slower than that of the unstimulated pulse, while positive amplitude stimuli always speed fronts up in the absence of adaptation.

5 Appendix

Here, we extract from Theorem A.1 of [12] the specific quantities used to compute the expressions in equations (3.37), (3.38) and present a brief summary of the corresponding calculations. For a more complete statement and discussion of this result, see [12].

The vector field for the slow q equation is given by $(\beta q - u)/c$. Using $u = g_\alpha(q)$, $\alpha \in \{L, R\}$ to denote the solutions of $q = F(u) - u$ as previously, we obtain the slow equation $\dot{q} = (\beta q - g_\alpha(q))/c$ on the slow manifold \mathcal{S} . From this expression, the corresponding adjoint equation is $\dot{q}^* = -(\beta/c)q^* + (1/c)g'_\alpha(q)q^*$, as given in equation (3.35). Note that this is the same equation as we obtain from system (3.32),(3.33), together with equation (3.34), in the singular limit $\kappa \rightarrow 0$.

To compute the jumps in the solution of (3.35), we need to find the left eigenvector w_j of the Jacobian matrix of the fast subsystem of (3.29) to which the jump take-offs are

tangent. The relevant matrix is given by

$$J = \begin{bmatrix} 1/c & -1/c & 0 \\ 0 & 0 & 1 \\ -F'(u) & 1 & 0 \end{bmatrix}.$$

If we let λ denote any eigenvalue of J , then a corresponding left eigenvector is given by

$$w_j = [c - c\lambda^2 \ \lambda \ 1]. \quad (5.42)$$

We shall see below that we will get the same jump directions and magnitudes no matter what nonzero constant multiple of w_j we use to compute them.

Remark 5.1 Note that the characteristic equation of J is $\lambda^3 - \lambda^2/c - \lambda + (1/c)(1 - F'(u)) = 0$, such that $\lambda = 1$ is an eigenvalue if and only if $F'(u) = 0$. If $F'(u) = 0$, then the eigenvalues of J are $\lambda = \pm 1, 1/c$. In fact, it can be shown that the eigenvalue corresponding to the left eigenvector governing the jump direction, in the limit $F'(u) \rightarrow 0$, tends to $\lambda = 1$. If this limit is reached, then the jump calculations break down, since $w_j = [0 \ 1 \ 1]$ results, but the only q^* dependence appears in the u^* equation.

Besides w_j , the jump calculations also use the vector f_q , corresponding to the vector of partial derivatives of the fast subsystem vector field with respect to q , given by $f_q = [1/c \ 0 \ 0]^T$. This quantity, equation (5.42), and equation (3.36) can be substituted into the following formula

$$\begin{aligned} c_j := w_j^T \left(\frac{q^*(\zeta_j^-)g(b_j) - 1}{w_j f_q g(b_j)} \right) &= \begin{bmatrix} c - c\lambda^2 \\ \lambda \\ 1 \end{bmatrix} \left(\frac{G(b_j)/G(a_j) - 1}{[c - c\lambda^2 \ \lambda \ 1] \begin{bmatrix} 1/c \\ 0 \\ 0 \end{bmatrix} [(\beta q - g_\alpha(q))/c]_{b_j}} \right) = \\ &= c \begin{bmatrix} c - c\lambda^2 \\ \lambda \\ 1 \end{bmatrix} \left(\frac{G(b_j) - G(a_j)}{(1 - \lambda^2)G(a_j)G(b_j)} \right), \end{aligned} \quad (5.43)$$

where $G(x) = (\beta q - g_\alpha(q))|_{(u,q,w,z)=x}$ as previously. Note that multiplication of w_j by a nonzero constant does not change this result, as claimed above.

Now, Theorem A.1 of [12] specifies that

$$q^*(\zeta_j^+) = q^*(\zeta_j^-) - f_q^T c_j = q^*(\zeta_j^-) - c \left(\frac{G(b_j) - G(a_j)}{G(a_j)G(b_j)} \right). \quad (5.44)$$

If we set $y^* = [u^* \ w^* \ z^*]^T$, then the theorem also gives $y^*(\zeta) = -(D_y g(\zeta) D_y f(\zeta)^{-1})^T q^*(\zeta)$ for $\zeta \neq \zeta_j$, where D_y denotes differentiation with respect to the fast variables (u, w, z) . At the jump points ζ_j , $y^*(\zeta)$ behaves as a δ -function, in the sense that

$$\int_{\zeta_j^-}^{\zeta_j^+} \dot{q}^*(\zeta) d\zeta = - \int_{\zeta_j^-}^{\zeta_j^+} f_q^T y^*(\zeta) d\eta. \quad (5.45)$$

From equation (5.44), the integral on the left hand side of equation (5.45) evaluates to $-f_q^T c_j$, such that equation (3.38) results from formula (5.43).

References

- [1] P. C. Bressloff, S. Folias, A. Pratt, and Y. Li. Oscillatory waves in inhomogeneous neural media. *Phys. Rev. Lett.*, 91:178101, 2003.
- [2] R. G. Casten, H. Cohen, and P. A. Lagerstrom. Perturbation analysis of an approximation to the Hodgkin-Huxley theory. *Quart. Appl. Math.*, 32:365–402, 1974/75.
- [3] R. D. Chervin, P. A. Pierce, and B. W. Connors. Periodicity and directionality in the propagation of epileptiform discharges across neocortex. *J. Neurophysiol.*, 60:1695–1713, Nov 1988.
- [4] B. W. Connors, D. J. Pinto, and A. E. Telfeian. Local pathways of seizure propagation in neocortex. *Int. Rev. Neurobiol.*, 45:527–546, 2001.
- [5] S. Coombes. Waves, bumps, and patterns in neural field theories. *Biol Cybern.*, 93:91–108, Aug 2005.
- [6] G. Ermentrout. Neural nets as spatio-temporal pattern forming systems. *Reports on Progress in Physics*, **61**:353–430, 1998.
- [7] G. B. Ermentrout and D. Kleinfeld. Traveling electrical waves in cortex: insights from phase dynamics and speculation on a computational role. *Neuron*, 29:33–44, Jan 2001.
- [8] G. B. Ermentrout and J. B. McLeod. Existence and uniqueness of travelling waves for a neural network. *Proc. Roy. Soc. Edinburgh Sect. A*, 123(3):461–478, 1993.

- [9] S. E. Folias and P. C. Bressloff. Breathing pulses in an excitatory neural network. *SIAM J. Appl. Dyn. Syst.*, 3(3):378–407 (electronic), 2004.
- [10] S. E. Folias and P. C. Bressloff. Stimulus-locked traveling waves and breathers in an excitatory neural network. *SIAM J. Appl. Math.*, 65(6):2067–2092 (electronic), 2005.
- [11] D. Golomb and Y. Amitai. Propagating neuronal discharges in neocortical slices: computational and experimental study. *J. Neurophysiol.*, 78:1199–1211, Sep 1997.
- [12] E. M. Izhikevich. Phase equations for relaxation oscillators. *SIAM J. Appl. Math.*, 60(5):1789–1804 (electronic), 2000.
- [13] K. Kishimoto and S. Amari. Existence and stability of local excitations in homogeneous neural fields. *J. Math. Biol.*, 7:303–318, 1979.
- [14] E. P. Krisner. The link between integral equations and higher order ODEs. *J. Math. Anal. Appl.*, 291(1):165–179, 2004.
- [15] D. J. Pinto and G. B. Ermentrout. Spatially structured activity in synaptically coupled neuronal networks. I. Traveling fronts and pulses. *SIAM J. Appl. Math.*, 62(1):206–225 (electronic), 2001.
- [16] D. J. Pinto, S. L. Patrick, W. C. Huang, and B. W. Connors. Initiation, propagation, and termination of epileptiform activity in rodent neocortex in vitro involve distinct mechanisms. *J. Neurosci.*, 25:8131–8140, Sep 2005.
- [17] K. A. Richardson, S. J. Schiff, and B. J. Gluckman. Control of traveling waves in the Mammalian cortex. *Phys. Rev. Lett.*, 94:028103, Jan 2005.
- [18] K. Takagaki, C. Zhang, J. Y. Wu, and M. T. Lippert. Crossmodal propagation of sensory-evoked and spontaneous activity in the rat neocortex. *Neurosci. Lett.*, 431:191–196, Feb 2008.
- [19] H. X. Wu, J. Y. and C. Zhang. Propagating waves of activity in the neocortex: what they are, what they do. *Neuroscientist*, 14:487–502, 2008.

- [20] W. Xu, X. Huang, K. Takagaki, and J. Y. Wu. Compression and reflection of visually evoked cortical waves. *Neuron*, 55:119–129, Jul 2007.